Bulletin of the Seismological Society of America, Vol. 87, No. 2, pp. 370–382, April 1997

Shallow Crustal Structure from Short-Period Rayleigh-Wave Dispersion Data in Southwestern Taiwan

by Jen-Kuang Chung and Yeong Tein Yeh

Abstract Strong ground motions in the period range of 1 to 5 sec observed in Taiwan in a dense network during the Tapu earthquake (M_L = 5.8) of 15 December 1993 were dominated by fundamental-mode Rayleigh waves. The shallow crustal structure beneath this network was determined from the group velocity dispersion data using standard inversion techniques. Results show that an alluvial layer with a thickness of only about 160 m exists over the sedimentary structure in the western coastal plain. A clear lateral variation in the shear-wave velocity along a cross section perpendicular to the western structural grain (Ho, 1982) was resolved.

For the purpose of retrieving the ground motions to confirm the proposed model, forward modeling with a two-dimensional finite-element method was used and agreed well with the observed seismograms when slightly lower velocities than those of the inversions were used. It is concluded that the velocity model estimated using group velocity data cannot definitively correspond to the real one at such short distances and in such a complex structure. On the basis of quantitative simulations, a very soft surface layer must be crucial in the interpretation of the slow wave trains with long duration and the rare prograde particle motions. The results suggest that these surface waves may be generated by the conversion of body waves at the boundary of the western coastal plain and foothills.

Introduction

Short-period surface waves are often used to infer the shear-wave velocity structure in the upper few kilometers of the crust. Many previous studies commonly used surface waves recorded from relatively shallow earthquakes (MacBeth and Burton, 1985; Niazi and Chun, 1989) and seismic explosions (Kafka and Reiter, 1987; MacBeth and Burton, 1986, 1988; Yao and Dorman, 1992). Nevertheless, some of these studies documented difficulties in extracting evident surface waves from the background noise in the period range of approximately 0.2 to 1 sec because only weak surface waves are excited by relative small sources.

Strong motions also include significant surface waves, especially in sediment-filled areas (Bard and Bouchon, 1980). Tanaka *et al.* (1980) showed that surface waves with a period of around 8 sec are predominant in seismograms recorded at a station in Tokyo on sediments during large earthquakes. Wang *et al.* (1989) analyzed well-developed wave trains across the strong-motion array in Taiwan (SMART-1) generated from two large earthquakes in the Hualien area of Taiwan and identified a group of weak dispersive fundamental-mode Rayleigh waves that they used to derive the subsurface velocity structure of the Ilan plain. Underlying most numerical and experimental studies, insight into underground structures down to the basement remains an important objective for seismic hazard reduction. With this purpose in mind, strong motion obtained from a dense network in southwestern Taiwan during the Tapu earthquake (M_L = 5.8) of 15 December 1993 was investigated. Distinct, well-dispersed later phases in the records were analyzed and interpreted as Rayleigh waves. The shear-wave velocity structure beneath this strong-motion network was derived by inversion, utilizing fundamental-mode group velocities in the period range of 1 to 5 sec.

Using the two-dimensional finite-element method, the forward modeling of the seismic waveforms was carried out to simulate the behavior of surface waves within sedimentary layers. The purpose was twofold: first, to understand the reasons by which these well-dispersed surface waves can generate in such a closed region, and second, to predict the strong ground motions during large earthquakes in the future.

Strong-Motion Records

For seismic hazard assessment and microzonation studies, the Taiwan Strong Motion Instrumentation Program (TSMIP) has been in operation since July 1991. The configuration of the very dense strong-motion network deployed

under one part of this program in southwestern Taiwan is depicted in Figure 1. The spacing between adjacent stations is about 5 km, but a more sparse distribution is common in the central range. Each station consists of a three-component accelerometer A-900 (Teledyne Geotech, 1993) or IDS-3602 (Terra Technology Corp., 1992) with a 16-bit resolution and a 96-db dynamic range, a setup that can record good quality digital data for even a small event. The net system response to acceleration for both types of accelerometer is almost flat from dc to 50 Hz (-3 db down). This network system has provided opportunities for researchers to investigate important seismic problems.

The Tapu earthquake ($M_L = 5.8$) of 15 December 1993 produced one of the most complete sets of strong-motion records. As determined from the shear waves, there is one relatively prolonged wave train in the vertical component of these seismograms (Fig. 2). These slow phases exhibit strong amplitudes in the period range of 1 to 5 sec observed at stations close to the western coast. The normal dispersion characteristics of these wave trains can be clearly identified. Such phases, in contrast, are seldom seen at the stations north or south of the epicenter in spite of the epicentral distances being in the same range as those in the western stations. The significant differences in waveform are visible when the records of stations CHY10, CHY46, CHY35, and CHY65 are compared with the others shown in Figure 2. If later wave trains are recognized as surface waves caused by the low-velocity sedimentary layer overlying the western coastal plain, the lack of surface waves should not seem surprising for stations located in the western foothills. This article focuses on the inversion to obtain the velocity structure using dispersion measured from vertical-component seismograms recorded at stations west of the source.

For the convenience of the analyses and simulations involved, displacement waveforms were integrated from accelerograms and then filtered by a high-pass filter with a cutoff frequency of 0.16 Hz, as shown in Figure 3. In this way, the described characteristics of waveforms have be-

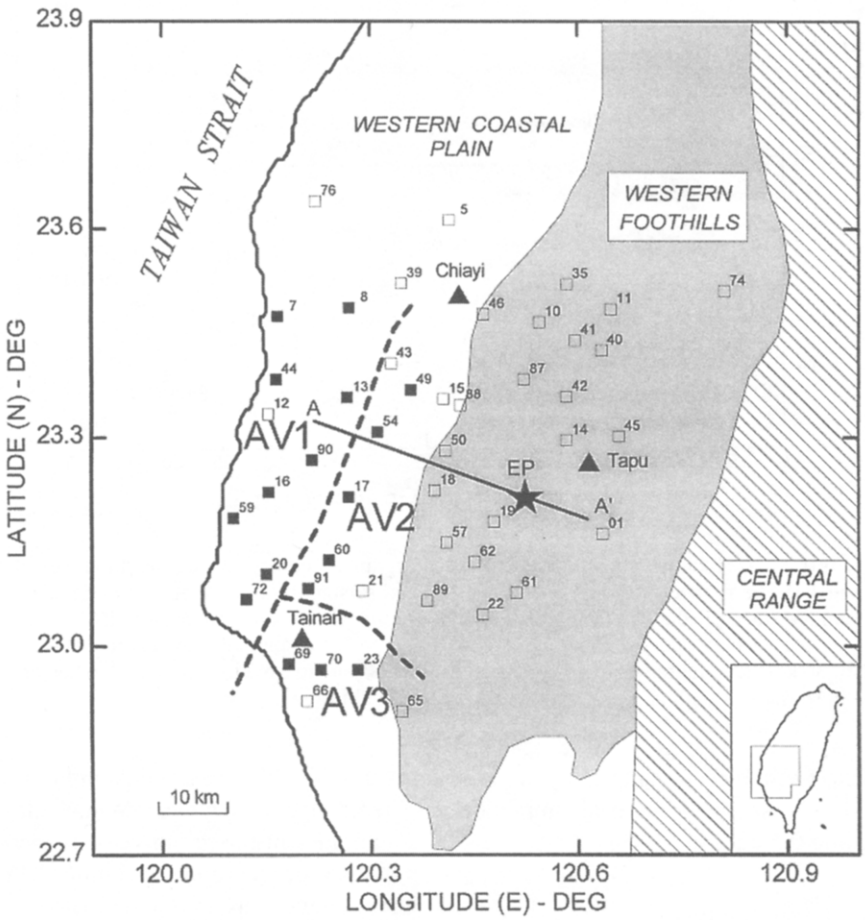

Figure 1. Strong-motion stations that recorded the ground motions during the Tapu earthquake of 15 December 1993. The epicenter is marked by a star (★). Only the code number of the station name is denoted: for example, "13" means "CHY13," and so on. The stations marked with solid squares recorded obvious surface waves that were observed and analyzed in this study. The dashed lines separate the region into three provinces, namely, AV1, AV2, and AV3.

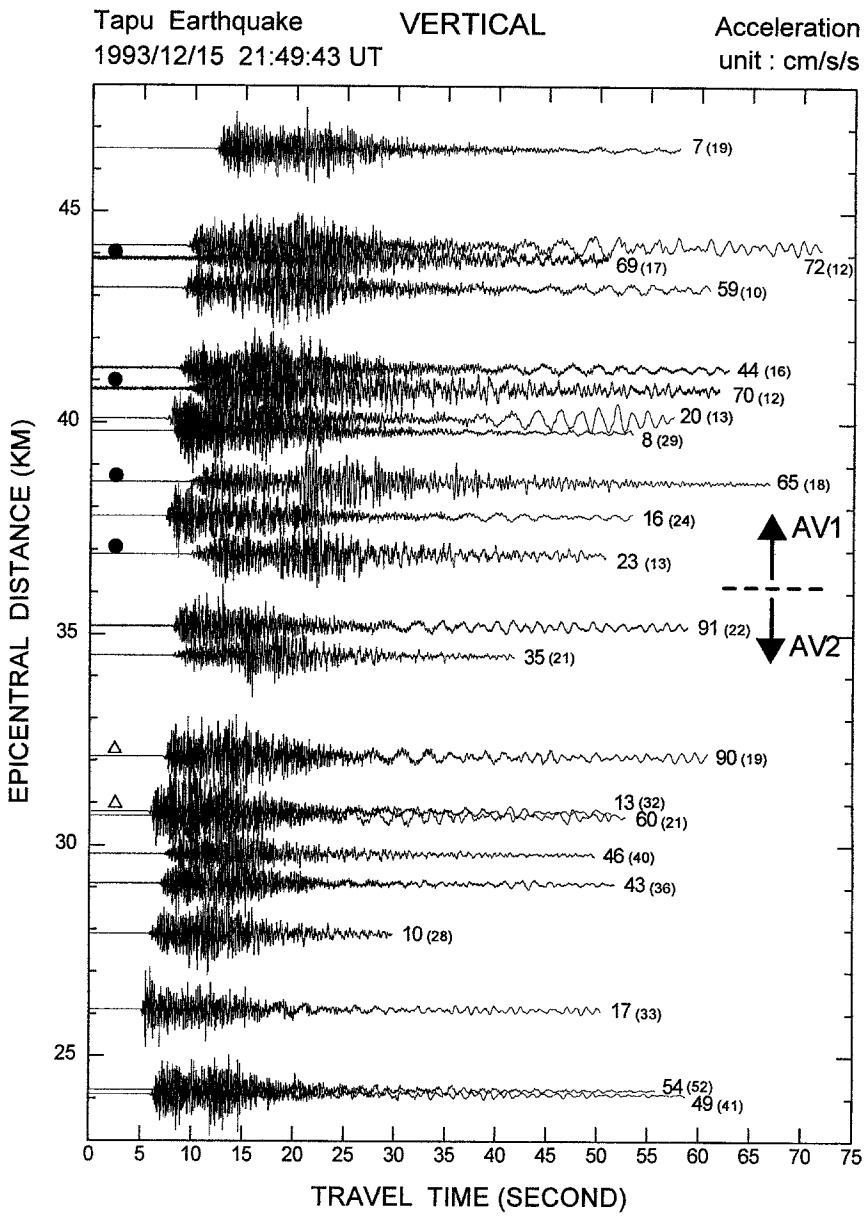

Figure 2. Examples of the vertical accelerograms recorded during the Tapu earthquake. The number attached to the end of each seismogram is the station code. The number in parentheses stands for the peak ground acceleration value in units of cm/sec/sec. The boundary dividing regions AV1 and AV2 is at about the epicentral distance of 36 km. The stations marked with a solid circle (●) are located in region AV3, whereas those marked with an open triangle (△) are located in region AV1.

come much more evident. Each trace, dominated by the surface waves, lasts for 20 to 35 sec, with the peak amplitude in some stations exceeding 0.5 cm.

Dispersion Analysis

Group velocities were derived using the multiple-filter technique of Dziewonski *et al.* (1969). The seismic signal was Fourier transformed and narrow bandpass filtered for a series of center frequencies. For each center frequency, the group arrival time was approximated by measuring the arrival time of the maximum amplitude of the envelope of the filtered signal. A typical contour diagram of instantaneous amplitudes in the group velocity–period plane is shown in Figure 4 for recordings at station CHY91. Normalization on the instantaneous amplitude matrix was performed individually for each frequency. Then, the dispersion curve could be obtained by following the signal maxima denoted as a reversed triangle in the diagram for each center frequency/period. The velocity interval selected to search the maxima of Rayleigh-wave energy at each period was 0.04 km/sec, which is narrow enough for distinct, well-dispersive wave

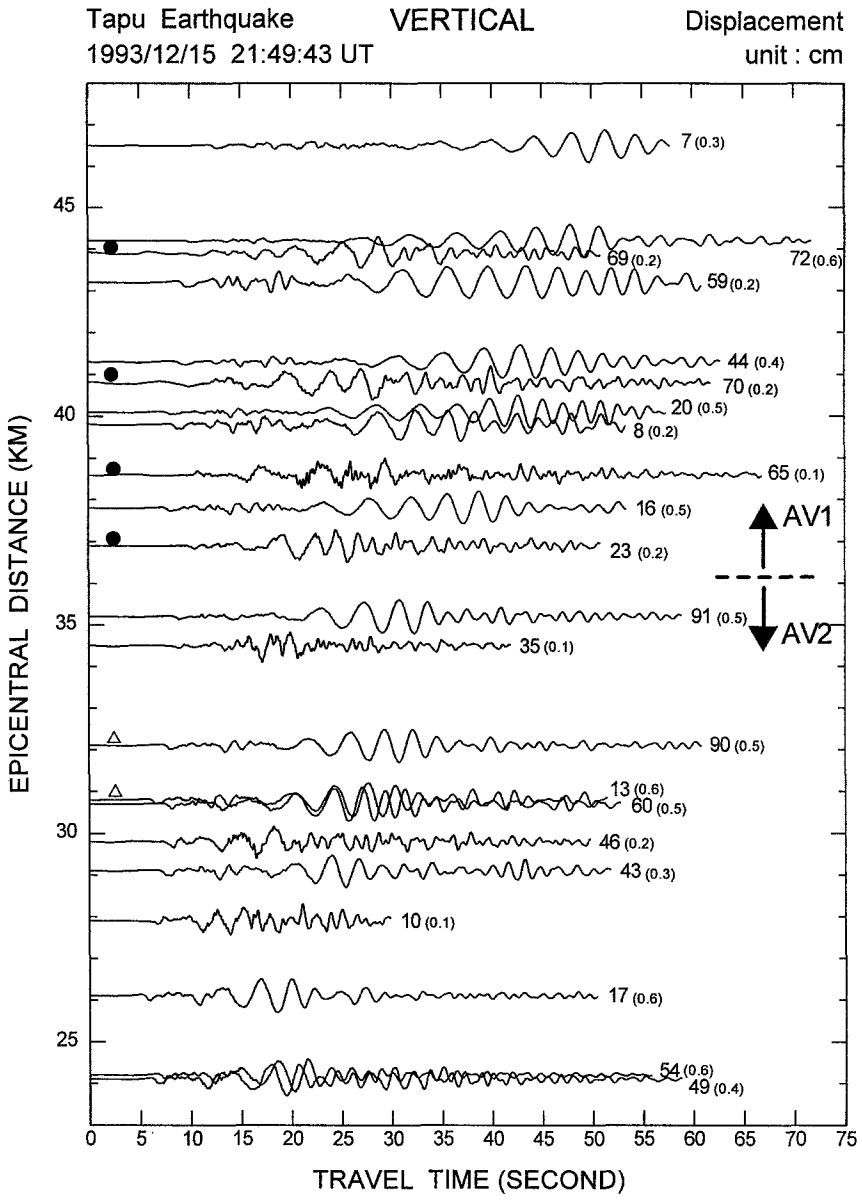

Figure 3. Integrated vertical displacement seismograms. The number attached to the end of each seismogram is the station code. The number in parentheses shows the peak value of the displacement in units of cm. These seismograms were filtered by a high-pass filter with a cutoff frequency of 0.16 Hz.

trains that mostly characterize the data used in this study. No treatment was performed to smooth the dispersion curves since several curves were grouped and averaged to obtain the velocity structure.

Seventeen dispersion curves were obtained, and all had typical shape for fundamental-mode Rayleigh waves propagating through a shallow structure with very low velocities in the most upper stratum. A noticeable phenomenon was the large variation in group velocity. In view of the variability expected in shallow structure, this is, to some degree, not surprising. However, a regular azimuthal change was not observed in the fanlike region covered by the propagation paths. Based on visual inspection, these dispersion curves can be classified into three groups as indicated in Figure 1 and separated by the dashed lines. With this division, the averaged group velocity increases from about 0.7 km/sec at a period of 1 sec to 1.4 km/sec at a period of 5 sec in region AV1 (Fig. 5). Less scattered dispersion values are, nevertheless, observed at periods shorter than 2 sec. This implies that the shear-wave velocity of the shallowest alluvium should be less than 1 km/sec. On the other hand, higher group velocities ranging from 0.8 to 1.8 km/sec for the same period range are obtained in region AV2 (Fig. 6). The velocities measured in this region show larger deviations than those in region AV1 for the entire period range of interest. In fact, the AV2 maximum variation of velocity reaches

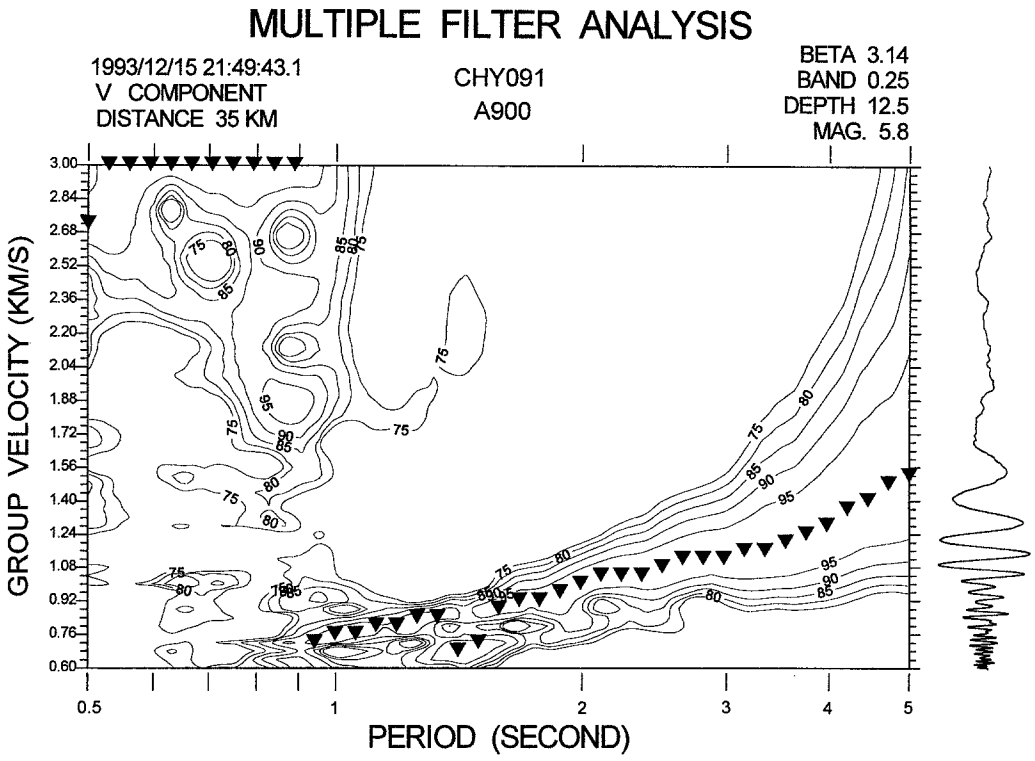

Figure 4. Multiple-filter analysis of the vertical-component displacement at station CHY91. The contours of relative energy higher than 75 db are drawn. The reversed solid triangles (▼) indicate the ridges of the filtered envelope for each period, respectively.

about 25% of the average velocity at a period of 5 sec. The first idea that comes to mind to explain this feature is that some error might have resulted from an incorrect recording time. The Global Positioning System (GPS) timing is standard equipment in each accelerometer, but when the routine maintenance reports were checked, a few stations were found to have had a 1-sec error about every 3 months. For stations with an epicentral distance of 30 km and an error of ± 1 sec in recording time, the maximum error in velocity estimation would be in the range of $\pm 2.4\%$ at a period of about 1 sec to $\pm 7.1\%$ at a period of 5 sec. This means that the large deviation must have mostly been due to lateral velocity variations. The three highest velocity curves (Fig. 7), measured by stations CHY23, CHY70, and CHY69, respectively, are coincidentally located in a very local area in the southwest of the plain. These stations were grouped in region AV3. One possible explanation of the observed pattern is that higher velocities were observed for paths parallel to the structural grain of the western foothills than for paths transversing the grain. Figure 8 shows that thrusting and folding in the western foothills is relatively shallow. Also, a surface of décollement underlying the imbricate fault zones can be recognized. This detachment plane separates the Neogene to late Oligocene rocks in the fold-thrust zone from the underlying basement (Ho, 1982). It can be assumed, therefore, that the NNE-trending Quaternary fault zone (Hsu and Chang, 1979) produced by the orogenic movement in the Plio-Pleistocene or early Pleistocene time seems to be the source of the lateral velocity variation behavior associated with the seismic waves. However, this will need to be verified using more data and convincing evidence in future studies.

Inversion for Shallow Structures

To obtain a model beneath the strong-motion network, a standard surface-wave inversion theory, first proposed by Backus and Gilbert (1970), was used. An interactive program developed by Russell *et al.* (1984) was used in the present study. This program inverts observed group velocities for the plane-layered shear-wave velocity structure and uses singular value decomposition (Lawson and Hanson, 1974) in the stochastic or differential form (Russell, 1987).

Since the upper-crustal structure is not known in this area, the detection of discontinuities or rapid gradients in velocity could be performed by setting several thin layers over the uncertain structure as an initial model and then inverting. A new model was obtained by putting the adjacent layers with almost the same velocity together. After this, the layer from the free surface to 1 km deep was divided into two or three layers independently, and the same procedure was also followed for the layer from 1 km to 3 km in depth.

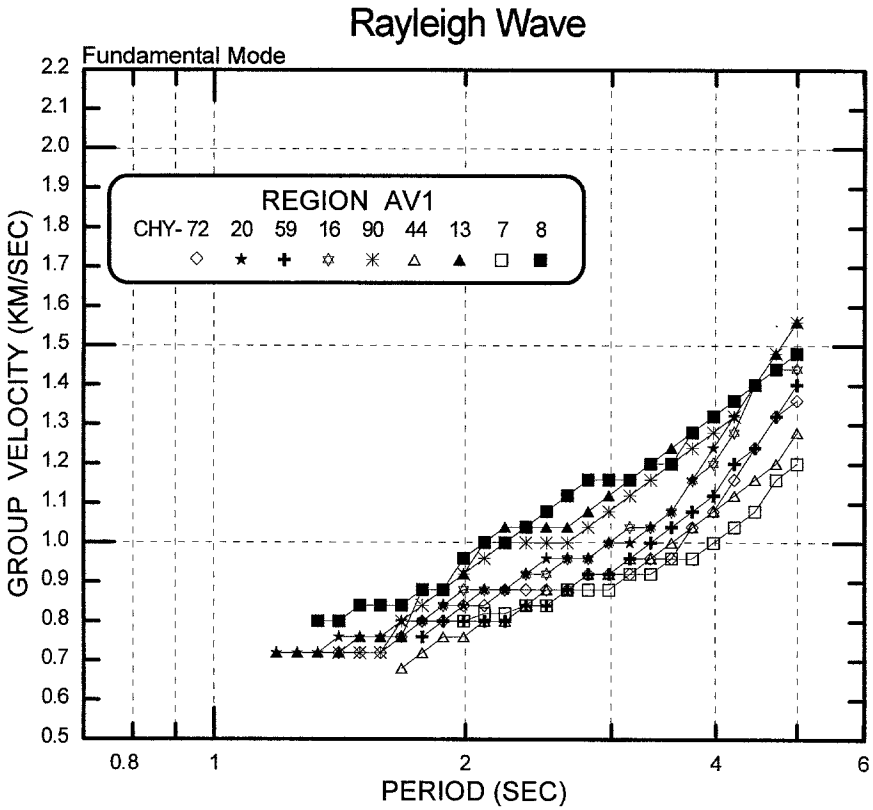

Figure 5. Dispersion curves of fundamental-mode Rayleigh waves for region AV1. Different symbols represent the corresponding station codes.

The velocity in the 3 to 4 km depth was assumed to be the same as that at the depth of 3 km, because the maximum resolved depth was about 3 km as determined by the data. Below the depth of 4 km, the *S*-velocity model from Ho (1994), which was derived from a three-dimensional travel-time inversion of body waves (*P* and *S* waves), was used and held fixed.

The short-period surface waves appeared to show great variation, as shown in the dispersed data and described in the previous section. This was due to local inhomogeneities within the shallow structure, and thus, in this article, a starting model was first found by inverting the averaged dispersion curve. A model corresponding to the individual dispersion curves was then derived utilizing the starting model during inversion. Finally, by taking the average of these models, the structure was obtained.

For each of the two regions, AV1 and AV2, the averaged group velocity dispersion values of the fundamental-mode Rayleigh wave were used to invert for velocity structure. Figures 9 and 10 show the comparisons between the observed curves and the theoretical curves as predicted by the inverted model. During the inversion scheme, both the shear-wave velocities and the layer thicknesses were iteratively inverted because these parameters are more sensitive to dispersion characteristics than the others (Bloch *et al.*, 1969). The empirical relationship between the density and the compressional velocity in rocks, proposed by Dobrin (1976), was used in this article. For sedimentary rocks, a variety of crystal structure and porosity were represented by the data. Accordingly, the mean curve fitting the scattered data was used, and it was found to be appropriate when compared with other results (Wang *et al.*, 1989, 1992). The velocity-inversion results (Figs. 11 and 12) indicate good resolution in the upper 3 km, except the surface layer of about 160 m thick in region AV1. The existence of unconsolidated alluvium in the western coastal plain is well known. In spite of having one low-rigidity cover layer with a thickness of about 250 m included in the model, the inverted shear velocities are between 0.70 and 0.82 km/sec for region AV1 and 0.9 km/sec for region AV2; however, some latent uncertainty still exists in region AV1 because of the poor resolving kernels brought on by the absence of associated observations for periods shorter than 1 sec. On the whole, considerable differences in velocity are constrained within the upper layers down to 4 km between these two provinces.

The inverted structures represented in Figures 11 and 12 became the initial models for the inversion of the individual structure for each station. In this step, the thicknesses of the layers were fixed during inversion. For each region, the final model was derived by averaging all of the models obtained using Rayleigh-wave dispersion data for individual

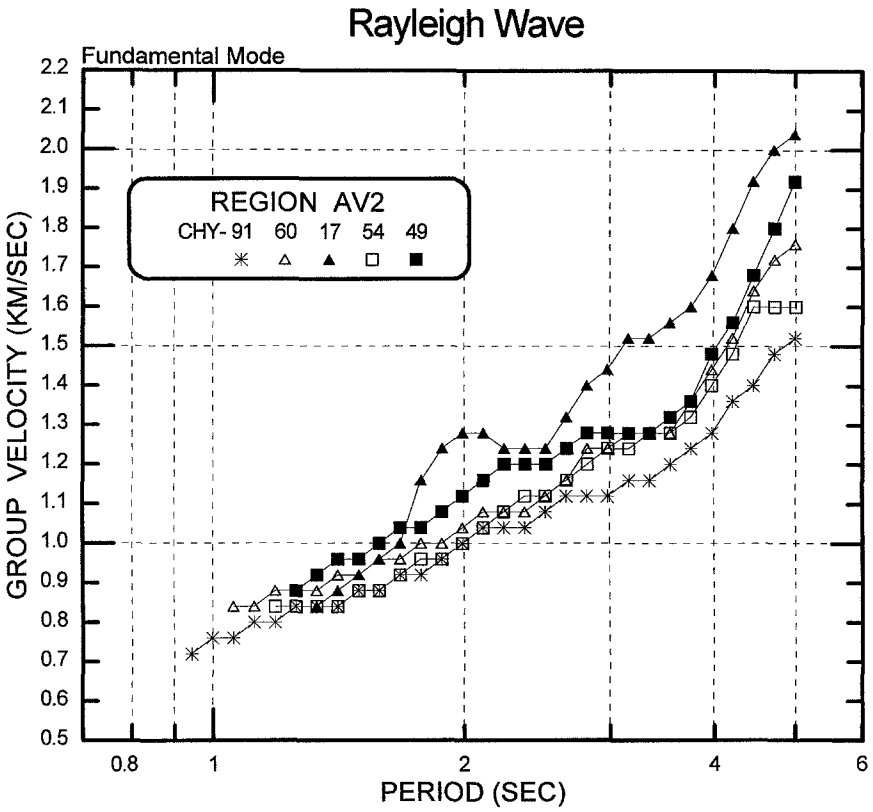

Figure 6. Dispersion curves of fundamental-mode Rayleigh waves for region AV2. Different symbols represent the corresponding station codes.

stations. Table 1 lists the resulting models. The shear-wave velocity of the top 160 m is 0.70 km/sec, whereas that of the next layer between 160 and 260 m is 0.82 km/sec in region AV1. Having analyzed the microtremors in the Chiayi and Tainan stations, Wang *et al.* (1992) proposed that the *S*-wave velocities of the top 200 m are in the range of 0.40 to 0.75 km/sec. The velocities obtained in this study were similar to those results. On the other hand, the interval *S*-wave velocity of 0.40 to 0.55 km/sec between 140 and 230 m was measured in the Tainan area using seismic reflection methods (Fang and Shih, 1994). For region AV2, only one layer with a shear-wave velocity of 0.90 km/sec in the top 290 m is derived. From 250 m down to about 800 m, the shear-wave velocities are 1.09 and 1.32 km/sec for regions AV1 and AV2, respectively. A relatively rapid change in velocity occurs at the boundary at about 800 m. Below this, down to 2100 m, the shear-wave velocities of 1.71 to 1.96 km/sec were mainly resolved from signals with a period of 2 to 4 sec that were predominant in all of the displacement waveforms. There was still a significant difference in velocity between 2100 and 4000 m for both regions, say 2.25 and 2.56 km/sec, respectively. Based on stratigraphic cross sections, they could have, however, belonged to the same Pliocene–Miocene strata unit (Ho, 1971; Tang, 1977). The deeper structure below 4000 m that is assumed to be the top of the pre-Miocene basement experienced no large perturbation when compared with the initial models. This also suggests that the data could not resolve the structure below such a depth when the propagation of the surface waves with the period range observed here were employed. A noticeable phenomenon is that the standard deviations of shear-wave velocity below the depth of 800 m derived from the data of region AV2 are generally larger than those from region AV1 (Table 1).

Numerical Modeling

To test the estimated velocity models, the finite-element method was employed to simulate the generation and propagation of short-period Rayleigh waves within the cross section in the northwestern direction passing through the epicenter (i.e., line AA′ in Fig. 1). Since the surface-wave inversion assumes a flat-layered structure, some modifications were made to construct a 2D model with one general feature being the edge of the sedimentary plain being against the foothill. Figure 13 represents the central part of the numerical model with a length of 200 km and a depth of 100 km. The structure on the foothill side, which partly corresponds to the central range, is divided into four layers over the half-space model based on the results of inversion. At the same time, two more low-velocity layers are modeled as the sedimentary plain that overlays the existing layers. The

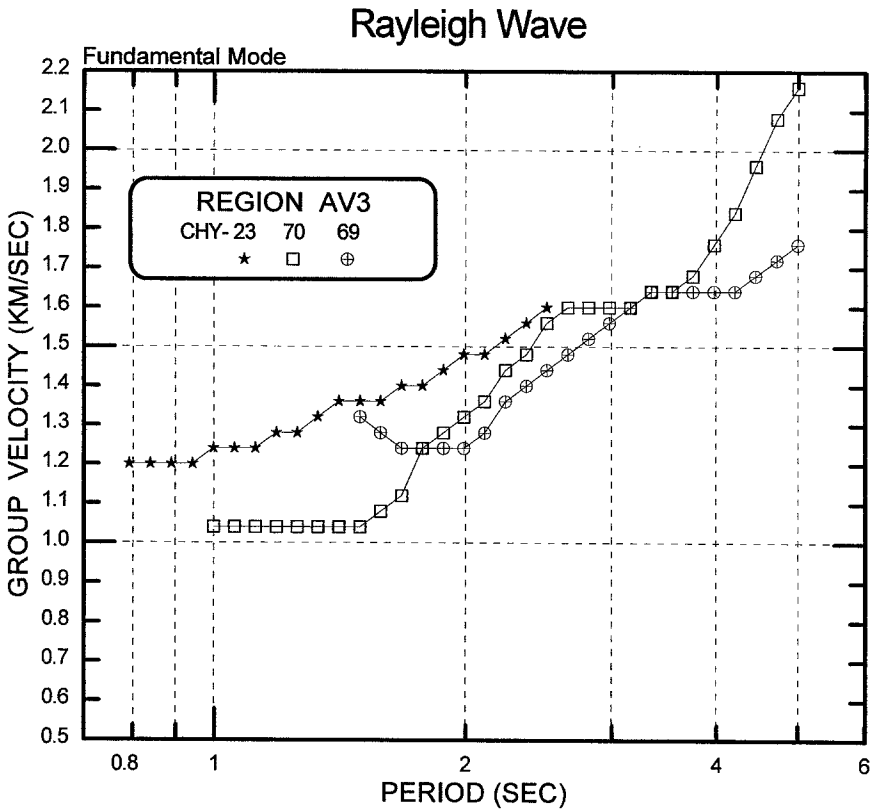

Figure 7. Dispersion curves of fundamental-mode Rayleigh waves for region AV3. Different symbols represent the corresponding station codes.

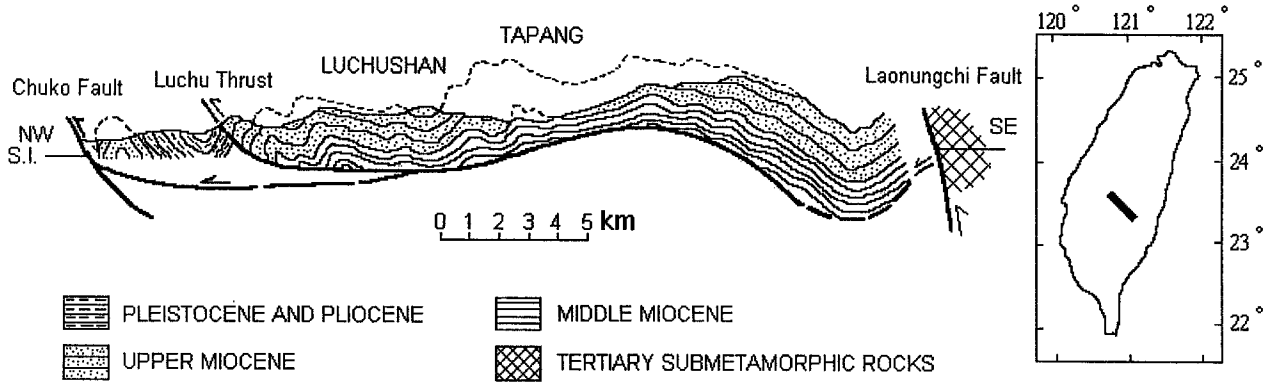

Figure 8. Structure section illustrating the gravity tectonics in the Alishan nappe of southern Taiwan (modified after Biq, 1969).

determination of the thickness of each layer was based on the AV1 model beneath the western coastal plain and the AV2 model under the western foothills. Two thin layers were allowed to merge into one layer.

The grid spacing of the model was 200 m, both horizontally and vertically. Therefore, the ability to resolve the signals with a frequency lower than 1 Hz could be achieved in compliance with the inherent characteristics of the finite-element calculation (Kuhlemeyer and Lysmer, 1973; Smith, 1975). The number of nodes exceeded 500,000, while the total degrees of freedom to be solved had a number of more than one million for the *P-SV* case in this study. To completely eliminate numerical reflections from the artificial boundaries, the absorbing boundary condition proposed by Smith (1974) was used. The dislocation source was simulated by the split-node technique (Melosh and Raefsky, 1981).

Based on the distribution pattern of the well-located aftershocks and the results of previous studies (Huang *et al,* 1994; Ho, 1994; Jiang, 1994), a west-inclined fault plane

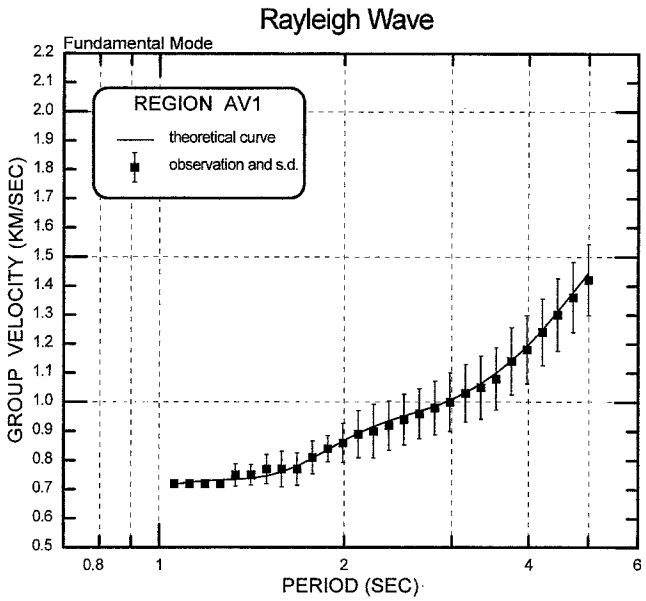

Figure 9. Comparison of the theoretical dispersion curve (solid line) and the averaged observations denoted by solid squares (■) with standard deviations for region AV1.

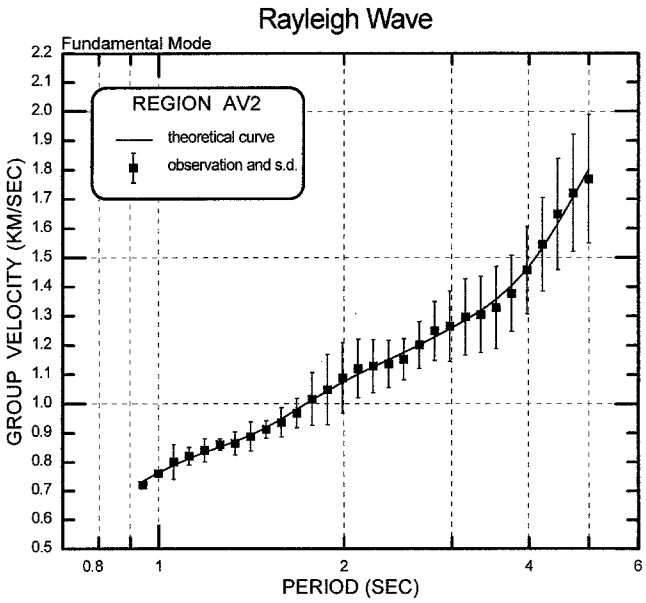

Figure 10. Comparison of the theoretical dispersion curve (solid line) and the averaged observations denoted by solid squares (■) with standard deviations for region AV2.

with a moderate dip angle was expected. The depth of 12.5 km was immediately announced by the Central Weather Bureau (CWB, 1993) using the HYPO71 routine program. A depth of 15 km, where the initial thrust-type rupture occurred and propagated upward with a rupture velocity of 2.45 km/sec for a width of 5 km along the fault, was chosen in this study. The source time function was a Gaussian function

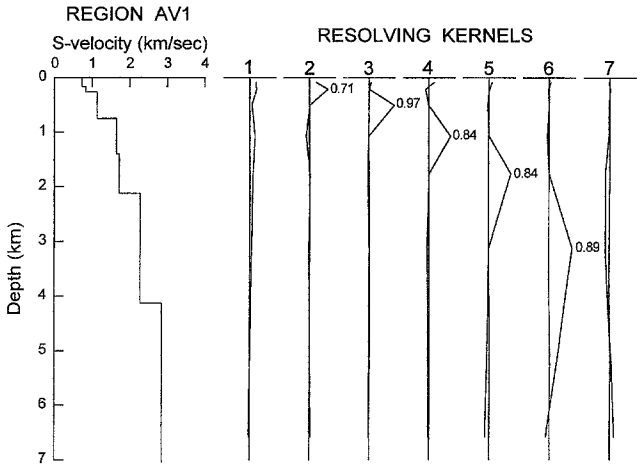

Figure 11. Initial shear-wave velocity model and the resolution kernels of region AV1 obtained by the inversion of the observed average group velocities.

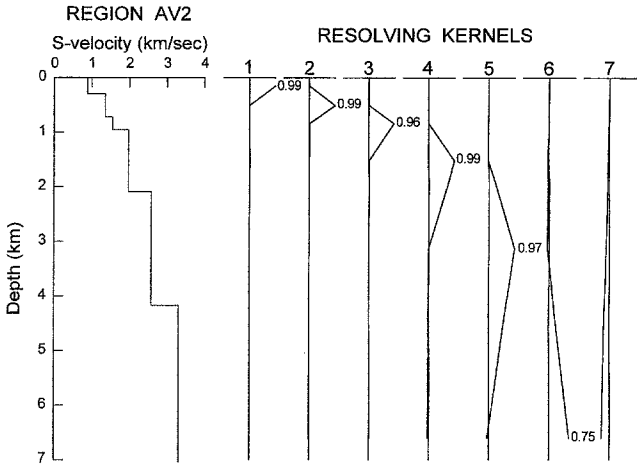

Figure 12. Initial shear-wave velocity model and the resolution kernels of region AV2 obtained by the inversion of the observed average group velocities.

Table 1

S-Velocity Models Obtained from Inversion of Averaged Group Velocity Data

Region AV1			Region AV2		
Thickness (km)	Velocity (km/sec)	SD (N = 9) (km/sec)	Thickness (km)	Velocity (km/sec)	SD (N = 5) (km/sec)
0.16	0.70	0.074	0.29	0.90	0.030
0.10	0.82	0.055	0.42	1.32	0.038
0.49	1.09	0.066	0.24	1.58	0.190
0.66	1.61	0.123	1.14	1.96	0.128
0.72	1.71	0.102	2.07	2.56	0.104
2.00	2.25	0.089	4.87	3.29	0.153
4.92	2.83	0.071	3.99	3.22	0.077
4.00	3.31	0.024	—	3.57	0.011
—	3.49	0.003			

*N: number of observations.

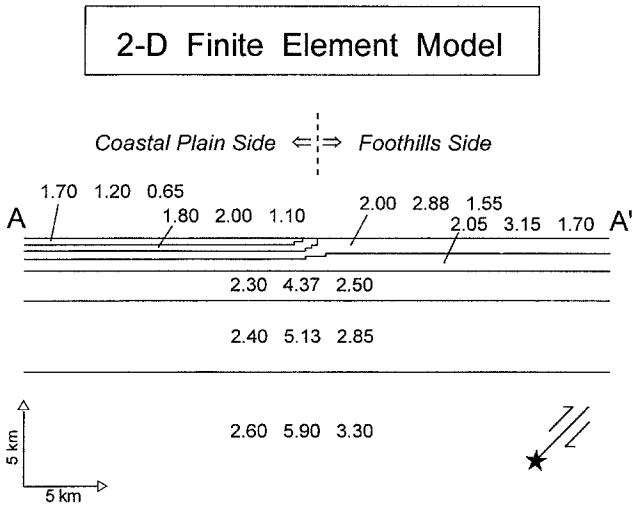

Figure 13. Two-dimensional finite-element model of the cross section AA′ depicted in Figure 1. The three numbers in each block show density, *P*-wave velocity, and *S*-wave velocity, respectively. A thrust-type dislocation fault is also shown. The star (★) indicates the initial rupture point.

with a predominant period of about 2 sec. However, a series of such functions in an orderly rupture along the fault plane can usually be combined to form a rough ramp function to simulate realistic rupturing. Therefore, a finite source with a dip of 45° was modeled in this study.

Figure 14 shows the comparisons between the observed waveforms and the synthetic seismograms in both the vertical and radial components. The agreement is good in most cases. The match in the amplitude and waveform is excellent, even at the high frequencies, for the closest station, CHY18, which was also simultaneously simulated for the purpose of examining the effects of source depth and fault dimension on the waveform.

The well-dispersed wave trains were synthesized in both components to fit the amplitude of observations. For the waves following the *S* waves, which can be identified in the time of 12 to 17 sec for stations CHY17 to CHY59, shown in Figure 14, the synthetic amplitudes in the radial component are significantly larger than those in the vertical component. This phenomenon does not seem to be so evident in the observed data. For comparison with the observed data, the larger amplitudes for the farther stations were synthesized. It should be explained that the calculations here do not include anelastic effects, which should have a principal effect on the amplitude of surface waves propagating in the sedimentary structure with a very low Q value (Joyner *et al.*, 1981; Frankel and Vidale, 1992).

Analytical solutions can show prograde motion in the fundamental-mode Rayleigh wave with the combination of a high shear velocity contrast and a high Poisson's ratio in the thin alluvium over the half-space model (Mooney and Bolt, 1966). In fact, this phenomenon was previously discussed by Jones *et al.* (1963) for an alluvial overburden. Such a special phenomenon of the prograde particle motions of the surface waves, it is noticed, did actually appear in the observed seismograms as well as in the synthetic results. In such a situation, a dominantly horizontal motion of the surface displacement could be expected.

Typical well-dispersed surface waves were only observed in the vertical component, not in the radial component. The synthetic seismograms (Fig. 14) also show this phenomenon and, in general, have good matches with the observations in both components. Phase misalignments in the vertical component of the first half of the surface wave trains are presented at stations CHY17, CHY44, and CHY59. For station CHY17, the synthetics show time delays in the surface wave trains. This was due to high group velocities in the observed data (Fig. 6). In contrast, the synthetics in station CHY44 and CHY59 are slightly advanced with regard to the observations that have slower velocities than the average dispersion curves (Fig. 5). These comparisons reflect a significantly heterogeneous lateral structure in the western coastal plain. In addition, the duration of shaking in the synthetic seismograms is shorter than that in the observations. This, though, is expected when 2D finite-element modeling is employed to simulate the 3D effects of seismic waves.

The slight differences in the *P*-wave arrival times could have been caused by the assumption made as to the lateral homogeneous layered structure below the depth of 9 km. Advances observed in near stations (i.e., CHY18 and CHY54) and delays in the others can actually be corrected by setting a higher velocity beneath the western coastal plain and contrarily a lower velocity in the source region. In so doing, the low-velocity zone would be very close to the one estimated by Ho (1994).

For insight into the generation of surface waves, the seismic profile of the vertical displacement records observed on the free surface is shown in Figure 15. More energy from the *S* waves is converted to surface waves at the edge of the alluvium located at the epicentral distance of 14 km. This high-velocity contrast structure also generates very slow phases with little dispersion (indicated by the arrows in Fig. 15). The velocity is about 0.34 km/sec. These slow phases can perhaps be identified as body waves bounded within the soft top layer and propagating like some kind of channel wave. In some observations, such as those at station CHY54, these later phases were found in the vertical component at 35 sec. Figure 16 shows the energy distribution of the surface waves in a vertical cross section at different times. Normal dispersion characteristics are clearly illustrated. The penetration depth of the surface waves trapped in the sedimentary basin is never deeper than 5 km in the short-period range.

Conclusions

Well-dispersed fundamental-mode Rayleigh waves generated by the Tapu earthquake of 15 December 1993 were

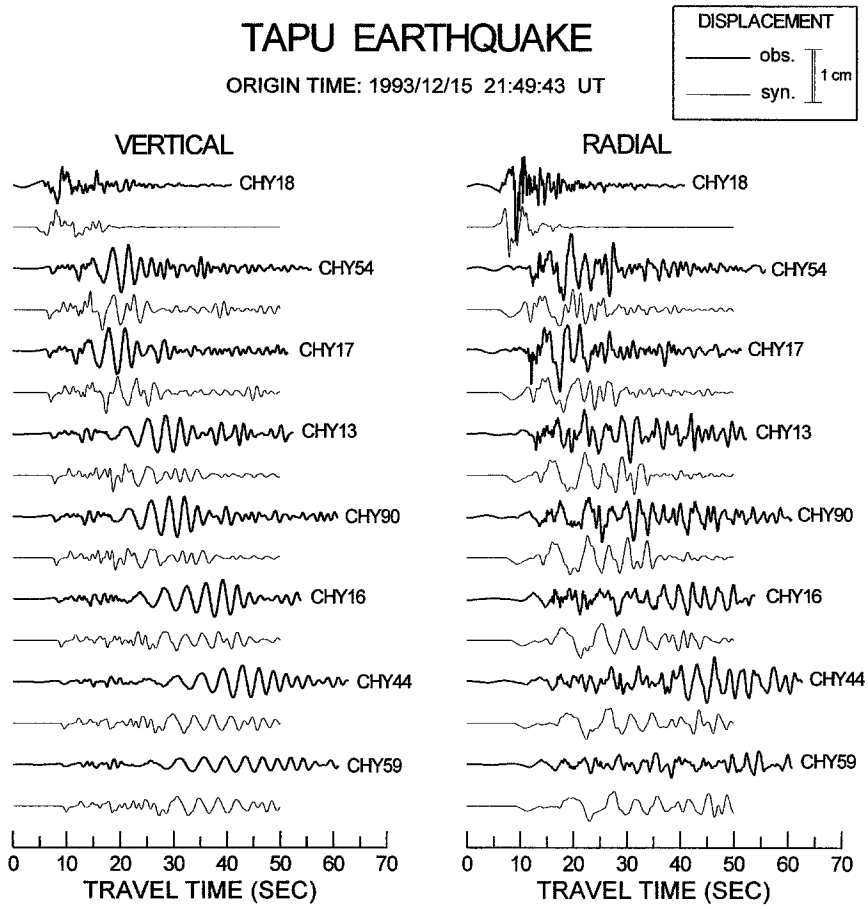

Figure 14. Comparisons of the synthetic seismograms (light traces) obtained from the finite-element simulation and the observations (heavy traces) in both the vertical and radial components.

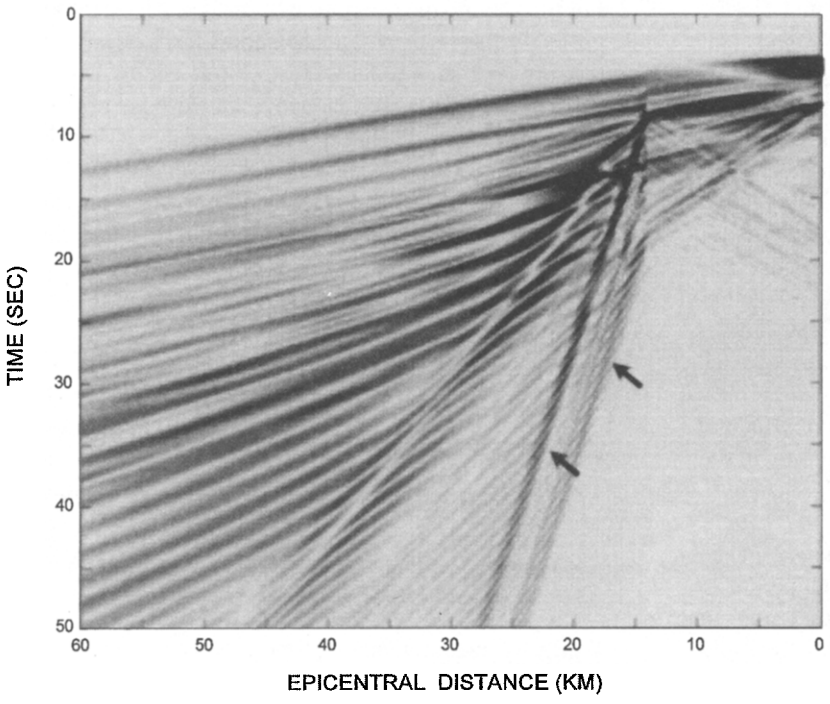

Figure 15. Synthetic seismic profile of vertical-component displacement on the free surface of the western side of the epicenter along direction AA′ depicted in Figure 13. The dark portions of the images had strong energy at that time. In contrast, the light portions had little or no energy at that time. The arrows indicate the slow phases discussed in the text.

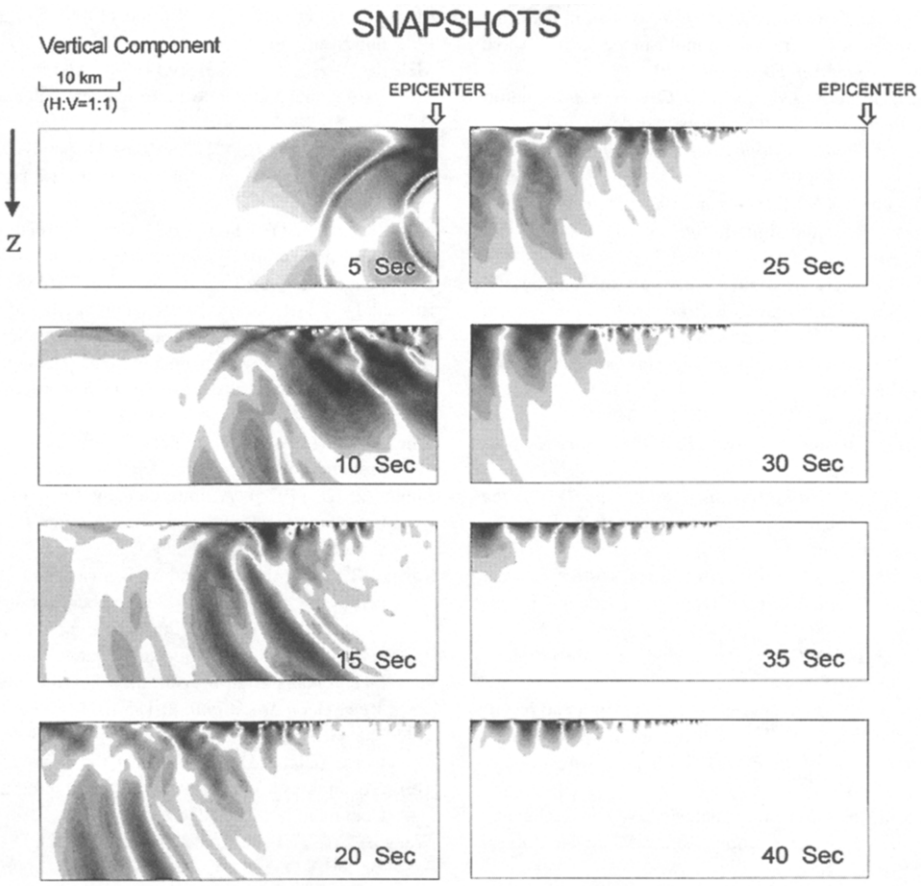

Figure 16. Fixed-time wave-field snapshots of the cross section with a depth of 20 km in the region on the western side of the epicenter.

recorded by a dense strong-motion network. Group velocity dispersion values were used to invert for the shear-wave velocity structure of the shallow crust in southwestern Taiwan. Results show that an alluvial layer with a thickness of only about 160 m existed over the sedimentary structure in the western coastal plain. Distinct lateral variations in the shear-wave velocity along the cross section perpendicular to the structural grain were estimated.

With the aim of confirming the derived structure, two-dimensional finite-element simulations were utilized to synthesize the strong ground motions. The match between the synthetic seismograms and the observations was good. The surprising fact that strong short-period surface waves were observed beyond the epicentral distance of about 25 km for an earthquake of 15 km in depth suggests that these surface waves may have been generated by the conversion of body waves at the boundary of the western coastal plain and foothills.

The amplitudes of the surface waves were larger in the horizontal component than in the vertical one. As shown by quantitative simulations, a very soft surface layer must be crucial in interpreting the slow wave trains with long duration as well as the rare prograde particle motions. As the velocities obtained using the surface waves represented an average over the paths from the epicenter to the recording stations, slightly lower velocities were readily given in the upper layers during simulations in this study. The *S*-wave velocity of about 0.65 km/sec in this layer, in summary, was determined and generally coincides with the models obtained from microtremors and reflection studies at comparable depths.

Acknowledgments

We are indebted to C. Y. Wang of National Central University for his surface-wave inversion code that became part of the procedure used here. We would like to thank T. L. Teng, T. C. Shin, J. W. Wang, G. K. Yu, Y. H. Yeh, and C. H. Hsieh for providing valuable comments. This work was supported by the National Sciences Council under Grant NSC84-2111-M-001-001.

References

Backus, G. and F. Gilbert (1970). Uniqueness in the inversion of inaccurate gross earth data, *Phil. Trans. Roy. Soc. London A* **266,** 123–192.

Bard, P.-Y. and M. Bouchon (1980). The seismic response of sediment-filled valleys. Part 2. The case of incident *P* and *SV* waves, *Bull. Seism. Soc. Am.* **70,** 1921–1941.

Biq, C. (1969). Role of gravitational gliding in Taiwan tectogenesis, *Bull. Geol. Surv. Taiwan* **20,** 1–39.

Bloch, S., A. L. Hales, and M. Landisman (1969). Velocities in the crust and upper mantle of southern Africa from multi-mode surface wave dispersion, *Bull. Seism. Soc. Am.* **59,** 1599–1629.

CWB (1993). *Seismological Bulletin: October to December, 1993,* Central Weather Bureau & Institute of Earth Sciences, Academia Sinica.

Dobrin, M. B. (1976). *Introduction to Geophysical Prospecting,* McGraw-Hill, New York, 630 pp.

Dziewonski, A. M., S. Bloch, and M. Landisman (1969). A technique for the analysis of transient seismic signals, *Bull. Seism. Soc. Am.* **59,** 427–444.

Fang, C.-K. and R.-C. Shih (1994). Preliminary study on the shallow velocity structure in Chiayi-Tainan area, in *Proc. of the Fifth Taiwan Symposium on Geophysics,* 217–226 (in Chinese).

Frankel, A. and J. Vidale (1992). A three-dimensional simulation of seismic waves in the Santa Clara Valley, California, from a Loma Prieta aftershock, *Bull. Seism. Soc. Am.* **82,** 2045–2074.

Ho, C.-S. (1971). The Tertiary basins of Taiwan, *Bull. Geol. Surv. Taiwan* **23,** 1–52.

Ho, C.-S. (1982). *Tectonic Evolution of Taiwan: Explanatory Text of the Tectonic Map of Taiwan,* The Ministry of Economic Affairs, Republic of China, 126 pp. (in Chinese).

Ho, M.-Y. (1994). Three dimensional velocity structure of western Taiwan, *Master's Dissertation,* National Central University, Chung-Li, Taiwan (in Chinese).

Hsu, T.-L. and H.-C. Chang (1979). Quaternary faulting in Taiwan, *Mem. Geol. Soc. China* **3,** 155–165.

Huang, B.-S., K.-C. Chen, and Y. T. Yeh (1994). Source depth and mechanism of the December 15, 1993 Tapu earthquake in Taiwan from strong motion records, *Proc. of the Fifth Taiwan Symposium on Geophysics,* 41–49.

Jiang, J.-S. (1994). Regional stress and strain analysis based on earthquake focal mechanisms, *Master's Dissertation,* National Taiwan University, Taipei, Taiwan (in Chinese).

Jones, G. H. S., G. T. Maureau, and S. A. Cyganik (1963). Air-blast coupling to prograde and retrograde surface waves, *J. Geophys. Res.* **68,** 4979–4987.

Joyner, W. B., R. E. Warrick, and T. E. Fumal (1981). The effect of Quaternary alluvium on strong ground motions in the Coyote Lake, California earthquake of 1979, *Bull. Seism. Soc. Am.* **71,** 1333–1349.

Kafka, A. L. and E. C. Reiter (1987). Dispersion of Rg waves in southeastern Maine: evidence for lateral anisotropy in the shallow crust, *Bull. Seism. Soc. Am.* **77,** 925–941.

Kuhlemeyer, R. L. and J. Lysmer (1973). Finite element accuracy for wave propagation problems (Technical note), *J. Soil Mech. Found. Div. Proc. ASCE* **99,** SM5, 421–427.

Lawson, C. L. and R. J. Hanson (1974). *Solving Least Squares Problems,* Prentice-Hall, New Jersey.

MacBeth, C. D. and P. W. Burton (1985). Upper crustal shear velocity models from higher mode Rayleigh wave dispersion in Scotland, *Geophys. J. R. Astr. Soc.* **83,** 519–539.

MacBeth, C. D. and P. W. Burton (1986). Propagation of 0.7–2.5 Hz Rayleigh waves in Scotland, *Geophys. J. R. Astr. Soc.* **84,** 101–120.

MacBeth, C. D. and P. W. Burton (1988). Surface waves generated by underwater explosions offshore Scotland, *Geophys. J.* **94,** 285–294.

Melosh, H. J. and A. Raefsky (1981). A simple and efficient method of introducing faults into finite element calculations, *Bull. Seism. Soc. Am.* **71,** 1391–1400.

Mooney, H. M. and B. A. Bolt (1966). Dispersive characteristics of the first three Rayleigh modes for a single surface layer, *Bull. Seism. Soc. Am.* **56,** 43–67.

Niazi, M. and K.-Y. Chun (1989). Crustal structure in the southern Bering Shelf and the Alaska Peninsula from inversion of surface-wave dispersion data, *Bull. Seism. Soc. Am.* **79,** 1883–1893.

Russell, D. R. (1987). Multi-channel processing of dispersed surface waves, *Ph.D. Dissertation,* St. Louis University, St. Louis, Missouri.

Russell, D. R., R. B. Herrmann, and H.-J. Hwang (1984). SURF: an interactive set of surface wave dispersion programs for analyzing crustal structure, *Earthquake Notes* **55,** 13.

Smith, W. D. (1974). A nonreflecting plane boundary for wave propagation problems, *J. Comp. Phys.* **15,** 492–503.

Smith, W. D. (1975). A finite element study of the effects of structural irregularities on body wave propagation, *Ph.D. Dissertation,* University of California, Berkeley.

Tanaka, T., S. Yoshizawa, and Y. Osawa (1980). Characteristics of strong earthquake ground motion in the period range from 1 to 15 seconds, *Proc. 7th World Conf. Earthquake Eng.* **2,** 609–616.

Tang, C.-H. (1977). Late Miocene erosional unconformity on the subsurface Peikang High beneath the Chaiyi-Yunlin coastal plain, Taiwan, *Mem. Geol. Soc. China* **2,** 155–168.

Teledyne Geotech (1993). Accelocorder III/A-900 operation & maintenance manual, Document no. 990-59400-9800.

Terra Technology Corp. (1992). IDS-3602 integrated digital seismograph, Document no. 95-310309.

Wang, C.-Y., Y. T. Yeh, and S.-J. Lin (1989). Dispersion of waves across the SMART-1 array, *Proc. Geol. Soc. China* **32,** 179–195.

Wang, C.-Y., S.-C. Wu, P.-L. Lu, L.-W. Hsu, and G.-S. Chang (1992). Investigation on microtremors near downhole stations of south central Taiwan, *Collected Papers of CWB/SOC* **3,** 215–234 (in Chinese).

Yao, P. C. and J. Dorman (1992). Short-period surface-wave dispersion and shallow crustal structure of central and eastern Tennessee, *Bull. Seism. Soc. Am.* **82,** 962–979.

Seismology Center
Central Weather Bureau
64, Kung Yuan Road
Taipei, Taiwan, Republic of China
(J.-K.C.)

Institute of Earth Sciences, Academia Sinica
P.O. Box 1-55
Nankang, Taipei, Taiwan, Republic of China
(Y.T.Y.)

Manuscript received 10 January 1995.